Microfluid Nanofluid (2012) 12:805–820
DOI 10.1007/s10404-011-0924-0

RESEARCH PAPER

Second-order gaseous slip flow models in long circular and noncircular microchannels and nanochannels

Zhipeng Duan

Received: 13 October 2011 / Accepted: 22 November 2011 / Published online: 10 December 2011

Abstract This paper significantly extends previous studies to the transition regime by employing the second-order slip boundary conditions. A simple analytical model with second-order slip boundary conditions for a normalized Poiseuille number is proposed. The model can be applied to either rarefied gas flows or apparent liquid slip flows. The developed simple models can be used to predict the Poiseuille number, mass flow rate, tangential momentum accommodation coefficient, pressure distribution of gaseous flow in noncircular microchannels and nanochannels by the research community for the practical engineering design of microchannels and nanochannels. The developed second-order models are preferable since the difficulty and "investment" is negligible compared with the cost of alternative methods such as molecular simulations or solutions of Boltzmann equation. Navier–Stokes equations with second-order slip models can be used to predict quantities of engineering interest such as the Poiseuille number, tangential momentum accommodation coefficient, mass flow rate, pressure distribution, and pressure drop beyond its typically acknowledged limit of application. The appropriate or effective second-order slip coefficients include the contribution of the Knudsen layers in order to capture the complete solution of the Boltzmann equation for the Poiseuille number, mass flow rate, and pressure distribution. It could be reasonable that various researchers proposed different second-order slip coefficients because the values are naturally different in different Knudsen number regimes. It is analytically shown that the Knudsen's minimum can be predicted with the second-order model and the Knudsen value of the occurrence of Knudsen's minimum depends on inlet and outlet pressure ratio. The compressibility and rarefaction effects on mass flow rate and the curvature of the pressure distribution by employing first-order and second-order slip flow models are analyzed and compared. The condition of linear pressure distribution is given.

Keywords Transition regime · Slip flow · Second-order model · Microchannels · Nanochannels · Pressure distribution · Mass flow rate · Knudsen's minimum

Z. Duan (✉)
University of Waterloo, Waterloo N2L3G1, Canada
e-mail: zpduan@uwaterloo.ca

Nomenclature

A	Flow area (m^2)
A_2	Second-order slip coefficient
a	Major semi-axis of ellipse or rectangle (m)
a	Base width of a trapezoidal, triangular, double-trapezoidal, or rhombic duct (m)
b	Minor semi-axis of ellipse or rectangle (m)
b	Height of a trapezoidal, triangular, double-trapezoidal, or rhombic duct (m)
c	Short side of a trapezoidal or double-trapezoidal duct (m)
D	Pipe diameter (m)
D_h	Hydraulic diameter $= \sqrt{A}(4\sqrt{A}/P)$
f	Fanning friction factor $= \tau/(\frac{1}{2}\rho\bar{w}^2)$
Kn	Knudsen number $= \lambda/D_h$
Kn^*	Modified Knudsen number $= Kn(2-\sigma)/\sigma$
L	Channel length (m)
$\mathcal{L}$	Arbitrary length scale
$\dot{m}$	Mass flow rate (kg/s)
m^*	Normalized mass flow rate
n	Correlation parameter
P	Total wetted perimeter (m)
Po	Poiseuille number $= \tau\mathcal{L}/\mu\bar{w}$

p	Pressure $(\mathrm{N/m^2})$
R	Specific gas constant $(\mathrm{J/kg\,K})$
Re	Reynolds number $= \bar{w}\mathcal{L}/\nu$
r	Dimensionless radius ratio $= r_i/r_o$
T	Temperature (K)
$\bar{w}$	Average velocity (m/s)
x, y	Cartesian coordinates (m)
z	Coordinate in flow direction (m)

Greek symbols

α_1, α_2	Parameters
δ_n	Eigenvalues
ε	Effective aspect ratio
λ	Molecular mean free path (m)
μ	Dynamic viscosity $(\mathrm{N\,s/m^2})$
ν	Kinematic viscosity $(\mathrm{m^2/s})$
σ	Tangential momentum accommodation coefficient
τ	Mean wall shear stress $(\mathrm{N/m^2})$
Ω	Half angle of annular sector (rad)

Subscripts

$\sqrt{A}$	Based upon the square root of flow area
D_h	Based upon the hydraulic diameter
i	Inlet
$\mathcal{L}$	Based upon the arbitrary length $\mathcal{L}$
ns	No-slip
o	Outlet

1 Introduction

Microchannels and nanochannels are the fundamental part of microfluidic and nanofluidic systems. Understanding the flow characteristics of micro/nanoscale flows is very important in determining pressure distribution, mass flow rate, pressure drop, heat transfer, and transport properties of the flow. The noncircular cross sections such as rectangular, isosceles triangular, trapezoidal, double-trapezoidal, rhombic, semi-circular, and elliptic are common channel shapes that may be produced by microfabrication. These cross sections have wide practical applications (Gad-el-Hak 2001; Nguyen and Wereley 2003; Karniadakis et al. 2005; Kandlikar et al. 2006; Li 2008).

The Knudsen number (Kn) relates the molecular mean free path of gas to a characteristic dimension of the duct. A typical mean free path of gas is approximately 70 nm at standard conditions. In the slip and transition regimes, the no-slip boundary conditions are not valid, and a kinetic boundary layer on the order of one mean free path (Cercignani 1988; Karniadakis et al. 2005), known as the ordinary Knudsen layer, starts to become dominant between the bulk of the fluid and the wall surface. The exact values for transition from one regime to another depend on the problem under consideration and the choice of length scale used to define the Knudsen number. In the previous works, various characteristic length scales have been employed (e.g. the radius or diameter for circular tubes, the height/half-height or hydraulic diameter/radius for annular, elliptical, rectangular, trapezoidal, double-trapezoidal, rhombic, and triangular channels).

As a result of the agreement between most liquid flow experimental data with characteristic dimensions larger than tens of microns and traditional theories derived assuming the no-slip boundary condition, today many textbooks of fluid mechanics and heat transfer neglect to mention that the no-slip and no-temperature-jump boundary conditions are only an assumption and cannot be derived from first principles. The common continuum flow (no-slip flow) is only a special case ($Kn \to 0$) of the present study.

Due to the lack of molecular-based theory of liquids, a dimensionless number similar to the Knudsen number is not commonly used for liquids. Thompson and Troian (1997) provided molecular dynamics simulations to quantify the liquid slip boundary condition dependence on the slip length and shear rate. The Navier boundary condition was employed to determine the degree of slip at a solid–liquid interface as the interfacial parameters and the shear rate change. When considering liquids, the molecular mean free path may be replaced by the slip length. The slip lengths reported experimentally span several orders of magnitude, from molecular lengths up to hundreds of nanometers with dependence on wetting conditions, surface roughness structure (shape and distribution), dissolved gas, surface charge, shear rate, and pressure. Recently, an investigation of the effects of wall stiffness, particles mass, and surface roughness on slip length was carried out by molecular dynamics simulations (Asproulis and Drikakis 2010a, b, 2011; Kalweit and Drikakis 2008). These studies may provide a better insight into the hydrodynamic boundary slip phenomena. If a nondimensional number similar to the modified Knudsen number (Kn^*) is defined for liquid slip flow, i.e., the ratio of slip length to a characteristic dimension of the flow field, the presently developed model for normalized Poiseuille number can be utilized to predict Poiseuille number, flow rate, and pressure drop (Chakraborty et al. 2008). To look at it from a slightly more general mathematical point of view, when no-slip condition on the solid surfaces is partially relaxed, the molecular mean free path and the term involving the accommodation coefficient $[\lambda(2-\sigma)/\sigma]$ and the slip length (λ_s) have the same mathematical meaning. Thompson and Troian (1997) indicated that there exists a nonlinear relationship between the amount of slip and a local shear rate at a solid surface at relatively higher shear rates. This suggests that the well-known linear Navier boundary condition may break down and can be

replaced by the general nonlinear second-order boundary condition in which $\Delta V = \lambda_s du/dy + A_{2L}\lambda_s^2(du/dy)^2$ where ΔV is the velocity difference between the solid and adjacent fluid and the liquid second-order slip coefficient A_{2L} can be obtained by comparing the model with numerical and experimental data. Therefore, the proposed second-order model provides a general picture of the momentum transport that occurs at liquid/solid or gas/solid interfaces. Liquid slip flow has emerged as an important research area. This has been motivated by its potential wide applications. Liquid slip is very important in nanofluidic devices with a superhydrophobic surface because it reduces the required pressure in pressure-driven flows and may be used to save energy (Tretheway and Meinhart 2002; Choi et al. 2003). The velocity slip and reduced liquid–solid contact of the superhydrophobic surfaces may lead to the temperature jump ($\Delta T \sim \lambda_s dT/dy$. and therefore additional thermal resistance) and reduction of the Nusselt number. However, the effects of velocity slip may win out the opposite effects of the temperature jump and thus improve the heat transfer rate for the same pumping power. This could be promising for the liquid cooling of microelectronic devices. The use of liquid slip is also a promising way to increase efficiency for energy conversion (e.g., the nanofluidic power generator).

In addition, Agrawal et al. (2009) and Rovenskaya and Croce (2010), respectively, numerically investigated gas flow in microchannels with a 90° bend and found that the pressure distribution and mass flow rate between the bent and straight long microchannels is nearly identical in the slip regime, and the similarity increases with an increase in Knudsen number. This indicates that the flow is less sensitive to the presence of the bend due to rarefaction effects of the gas and thus furnishes a desirable advantage in the design of microdevices. For example, we can use impingement flow to replace parallel flow in microchannel heat sinks to enhance heat transfer because the thermal performance of microchannel heat sinks in impingement flow exceeds that of similar heat sinks in parallel flow (this is attributed to the synergistic enhancement of velocity field and temperature field). Therefore, all the developed models (Poiseuille number, pressure distribution, mass flow rate, and pressure drop) for straight microchannels can be utilized for bent microchannels within negligible difference. This could be important because of a shortage of information for bent circular and noncircular microchannels in the literature.

2 Literature review

The small length scales commonly encountered in microfluidic devices suggest that rarefaction effects are important. For example, experiments conducted by Pfahler et al. (1990), Arkilic et al. (1994, 1997), Harley et al. (1995), Choi et al. (1991), Pong et al. (1994), Araki et al. (2000), Zohar et al. (2002), Jang and Wereley (2004), Hsieh et al. (2004) on the transport of gases in microchannels confirm that continuum analyses are unable to predict flow properties in micro-sized devices.

Arkilic et al. (1994, 1997) studied helium flow through microchannels and found significant reduction in the Poiseuille number. The reduction may be due to the slip flow regime, as according to the flow regime classification by Schaaf and Chambre (1958), the flows investigated by Arkilic et al. are mostly within the slip flow regime, only bordering the transition regime near the outlet.

Maurer et al. (2003) conducted experiments for helium and nitrogen flow in 1.14 μm deep 200 μm wide shallow microchannels. Flowrate and pressure drop measurements in the slip and early transition regimes were performed for averaged Knudsen numbers extending up to 0.8 for helium and 0.6 for nitrogen. The authors also provided estimates for second-order effects and found the upper limit of slip flow regime as the averaged Knudsen number equals 0.3 ± 0.1.

Aubert and Colin (2001) studied slip flow in rectangular microchannels using the second-order boundary conditions proposed by Deissler (1964). In a later study, Colin et al. (2004) presented experimental results for nitrogen and helium flows in a series of silicon rectangular microchannels. The authors proposed that the second-order slip flow model is valid for Knudsen numbers up to about 0.25.

Ewart et al. (2006, 2007a) measured mass flow rate of isothermal gaseous slip flow in microtubes. The principle of their measurement is similar to that of Maurer et al. (2003). The measured values were compared with analytical solutions and satisfactory results were obtained. The authors show that the second-order effects could exist for average Knudsen numbers larger than 0.1.

The analytical study of internal flows with slip previously has been confined to simple geometries (Kennard 1938; Ebert and Sparrow 1965; Sreekanth 1969; Mitsuya 1993), beginning with early efforts in the kinetic theory of gases. In an effort to extend the range of applicability of slip flow boundary conditions to the transition regime, some researchers (Karniadakis et al. 2005; Xue and Fan 2000; Jie et al. 2000; Li et al. 2000; Hadjiconstantinou 2006; Reese and Zhang 2009; Cercignani and Lorenzani 2010; Pitakarnnop et al. 2010) have proposed some second-order modifications and methods recently; to mention but a few. However, there are large variations in the second-order slip coefficient (Karniadakis et al. 2005; Barber and Emerson 2006). The boundary conditions derived by Deissler (1964), and the boundary conditions suggested by Karniadakis et al. (2005) are the commonly applied second-order slip boundary condition models, which also provide temperature jump boundary conditions. Although

many second-order models have been proposed, and some have been demonstrated useful in increasing the range and accuracy of the slip boundary condition representation of rarefaction either experimentally or numerically, there is insufficient experimental data to validate the use of any particular second-order model over another at present.

We may now briefly examine the first-order slip flow solution for rectangular ducts. The friction factor and Reynolds number product was presented by Ebert and Sparrow (1965) and Duan and Muzychka (2007a):

The ratio of minor and major axes is ε. The constant σ denotes tangential momentum accommodation coefficient,

$$fRe_{\sqrt{A}} = \frac{2\left(-\frac{A}{P}\frac{\mathrm{d}p}{\mathrm{d}z}\right)\sqrt{A}}{\mu\bar{w}} = \frac{2}{\sqrt{\varepsilon}(1+\varepsilon)\sum_{n=1}^{\infty}\frac{\varepsilon\sin^2\delta_n}{\delta_n^4(\delta_n+\sin\delta_n\cos\delta_n)}\left[\frac{\delta_n}{\varepsilon}-\frac{\sin h\left(\frac{\delta_n}{\varepsilon}\right)}{\cos h\left(\frac{\delta_n}{\varepsilon}\right)+\frac{4}{1+\varepsilon}Kn^*\delta_n\sin h\left(\frac{\delta_n}{\varepsilon}\right)}\right]}. \quad (1)$$

It may be pointed out that most of the following statements, formulas, and charts are valid only for long ducts. The fluid flow behavior in the developing region differs from that in the fully developed region. The parameter $L/(D_{\mathrm{h}}Re)$ is always a significant parameter in internal fluid flows. The flow behaves differently and is dominated by the different mechanisms as the parameter $L/(D_{\mathrm{h}}Re)$ changes. This effect of developing region is significant if the microchannels are short. Details on slip flow in the developing region can be found in Duan and Muzychka (2010). Generally, the entrance region effects are less than 2% and can be neglected as $L/(D_{\mathrm{h}}Re) \geq 1$.

3 Second-order models

In the fluid flow and heat transfer literature the convention is to use the hydraulic diameter. However, for noncircular ducts, the question always arises of what to use as the correct length scale. Although it is customary to use the hydraulic diameter, this choice is widely believed to be inappropriate. For noncircular geometries, it is desirable to eliminate or reduce the effects of geometry such that the general trends for all duct shapes may be easily modeled. Muzychka and Yovanovich (2002), Duan and Muzychka (2007a, 2010), and Duan and Yovanovich (2010) showed that the square root of the cross-sectional area was a more appropriate characteristic length scale than the hydraulic diameter for non-dimensionalizing the laminar no-slip and slip flow data. Recently, Duan (2012) reached the same conclusion for turbulent flow. When $\sqrt{A}$ is used, the effect of duct shape becomes *minimized*, and all of the data can be predicted using a simple model based on the solution for the rectangular duct. The definition of effective aspect ratio is summarized in Table 1.

which is usually between 0.87 and 1 (Rohsenow and Choi 1961). The eigenvalues, δ_n, can be obtained from $\delta_n \tan\delta_n = (1+\varepsilon)/(4Kn^*)$. It can also be demonstrated that Eq. 1 reduces to its no-slip flow limits as $Kn^* \to 0$ (Duan and Muzychka 2007a):

$$\left(fRe_{\sqrt{A}}\right)_{\mathrm{ns}} = \frac{12}{\sqrt{\varepsilon}(1+\varepsilon)\left[1-6\sum_{n=1}^{\infty}\frac{\varepsilon}{\delta_n^5}\tanh\left(\frac{\delta_n}{\varepsilon}\right)\right]} \quad (2)$$

Examination of the single-term solution reveals that the single-term approximation is accurate enough for engineering applications. The largest difference occurs when $\varepsilon = 1$, which is less than 0.7%. When greater accuracy is desired, two terms are definitely enough due to rapid convergence. Considering only the two terms of the series, Eq. 2 gives:

$$\left(fRe_{\sqrt{A}}\right)_{\mathrm{ns}} = \frac{12}{\sqrt{\varepsilon}(1+\varepsilon)\left[1-\frac{192\varepsilon}{\pi^5}\left(\tanh\left(\frac{\pi}{2\varepsilon}\right)+\frac{1}{243}\tanh\left(\frac{3\pi}{2\varepsilon}\right)\right)\right]} \quad (2a)$$

The theory for continuum, slip, and free molecular regimes is generally well developed (Kennard 1938; Schaaf and Chambre 1958; Cercignani 1988; Gad-el-Hak 2001; Karniadakis et al. 2005; Kandlikar et al. 2006; Sone 2007; Li 2008). However, the theoretical basis and a definitive picture of the transition regime is not very clear. The transition regime is the most complicated domain for modeling.

Analytical models derived using the first-order slip boundary conditions have been widely shown to be relatively accurate up to Knudsen numbers of approximately 0.1. For higher values of Knudsen number, the validity of Navier–Stokes equations to rarefied gases can be improved by using second-order slip boundary conditions and appropriate selection of the slip coefficients. The results

Table 1 Definitions of effective aspect ratio

Geometry	Effective aspect ratio
Regular polygons	$\varepsilon = 1 N \geq 4$
Simple singly-connected	$\varepsilon = \frac{b}{a}$
Trapezoid (including approximate trapezoid)	$\varepsilon = \left[\left(\frac{2b}{a+c}\right)^n + \left(\frac{a+c}{2b}\right)^n\right]^{-1/n}$ $n = 1.7$
Arbitrary triangle (including approximate triangle)	$\varepsilon = \left[\left(\frac{2b}{a}\right)^n + \left(\frac{2a}{b}\right)^n\right]^{-1/n}$ $n = 0.53$
Double-trapezoid	$\varepsilon = \left[\left(\frac{a+c}{2b}\right)^n + \left(\frac{1+\frac{c}{a}}{\frac{2a}{b}}\right)^n\right]^{-1/n}$ $n = 2.8$
Rhombus	$\varepsilon = \left[\left(\frac{2b}{a}\right)^n + \left(\frac{2a}{b}\right)^n\right]^{-1/n}$ $n = 0.68$
Annular sector	$\varepsilon = \frac{1-r}{\Omega(1+r)}$

reduce to first-order results upon neglecting the second-order slip term as expected. In recent years, there has been some success in the implementation of second-order slip boundary conditions to extend the Navier–Stokes equations into the transition regime. It is generally accepted that second-order slip models can be used with considerable success provided the appropriate (well-founded) second-order slip coefficient is chosen (Hadjiconstantinou 2006; Sone 2007; Cercignani and Lorenzani 2010; Lorenzani 2011; Karniadakis et al. 2005, to mention but a few).

The developed second-order slip models are preferable since the difficulty and "investment" is completely negligible compared with the cost of alternative methods such as molecular simulations or solutions of Boltzmann equation, which require great computational effort that is not justified in practical calculations. Extending the range of applicability of the Navier–Stokes equations beyond first-order slip flow within acceptable error is desirable due to the remarkable simplicity and significant computational efficiency. For this reason, a variety of researchers have attempted to develop high-order models which can be used in the transition regime. Hadjiconstantinou (2006) verified that when the Knudsen layers essentially cover the whole physical domain, the second-order slip remains reasonably accurate in predicting the stress field and bulk flow velocity. It appears that the underlying Navier–Stokes constitutive relation remains robust up to $Kn \approx 0.4$. Even though the Kundsen layers penetrate to the middle of the physical domain at higher Knudsen numbers, the second-order slip model remains quantitatively accurate up to $Kn \approx 1$.

In addition, there is no consensus as to whether the term involving the accommodation coefficient (i.e., $(2-\sigma)/\sigma$) should be associated with both the first- and second-order slip coefficients or whether it should only be associated with the first-order term. This is of little concern for fully diffusive boundaries but may result in significant discrepancies in the case of incomplete momentum accommodation. It is assumed that the term involving the accommodation coefficient $[(2-\sigma)/\sigma]$ is associated with both the first- and second-order slip coefficients for convenience in the present paper, which is consistent with Karniadakis et al. (2005), Xue and Fan (2000), Jie et al. (2000), and Cercignani and Lorenzani (2010).

Aubert and Colin (2001) completed an excellent work to obtain the velocity distribution with Deissler second-order slip boundary conditions in rectangular microchannels. Aubert and Colin showed that the velocity distribution with first-order slip boundary conditions, in the form of a single Fourier series, does not converge with second-order boundary conditions. Therefore, they proposed a new form based on a double Fourier series (Carslaw and Jaeger 1959). As there is currently no sufficient experimental data to validate the application of any particular second-order model over another, the second-order slip boundary conditions may be written in the following general form (Aubert and Colin 2001):

$$w|_{y=b} = -\lambda \frac{2-\sigma}{\sigma} \left.\frac{\partial w}{\partial y}\right|_{y=b} - A_2 \lambda^2 \left(\frac{2-\sigma}{\sigma}\right)^2 \left(\left.\frac{\partial^2 w}{\partial y^2}\right|_{y=b} + \frac{1}{2}\left.\frac{\partial^2 w}{\partial x^2}\right|_{y=b}\right) \tag{3}$$

$$w|_{x=a} = -\lambda \frac{2-\sigma}{\sigma} \left.\frac{\partial w}{\partial x}\right|_{x=a} - A_2 \lambda^2 \left(\frac{2-\sigma}{\sigma}\right)^2 \left(\left.\frac{\partial^2 w}{\partial x^2}\right|_{x=a} + \frac{1}{2}\left.\frac{\partial^2 w}{\partial y^2}\right|_{x=a}\right) \tag{4}$$

The velocity distribution (Aubert and Colin 2001) and average velocity are

$$w(x,y) = -\frac{b^2}{\mu}\frac{\mathrm{d}p}{\mathrm{d}z}\left[\sum_{i,j=1}^{\infty} A_{ij} \cos\left(\varphi_i \frac{x}{a\varepsilon}\right) \cos\left(\psi_j \frac{y}{b}\right) + 2A_2 \frac{4}{(1+\varepsilon)^2} Kn^{*2}\right] \tag{5}$$

$$\bar{w}(x,y) = -\frac{b^2}{\mu}\frac{\mathrm{d}p}{\mathrm{d}z}\left[\sum_{i,j=1}^{\infty} A_{ij} \frac{\varepsilon \sin\left(\frac{\varphi_i}{\varepsilon}\right) \sin\psi_j}{\varphi_i \psi_j} + 2A_2 \frac{4}{(1+\varepsilon)^2} Kn^{*2}\right] \tag{6}$$

where φ_i and ψ_j are eigenvalues and can be obtained from the following equations, respectively (Aubert and Colin 2001):

$$\frac{4}{1+\varepsilon} Kn^* \varphi_i \tan\frac{\varphi_i}{\varepsilon} + 2A_2 \frac{4}{(1+\varepsilon)^2} Kn^{*2} \varphi_i^2 = 1 \tag{7}$$

$$\frac{4}{1+\varepsilon}Kn^{*}\psi_j\tan\psi_j+2A_2\frac{4}{(1+\varepsilon)^2}Kn^{*2}\psi_j^2=1 \tag{8}$$

and

$$\alpha_1=12-10.598\varepsilon+8.654\varepsilon^2-2.231\varepsilon^3 \tag{13}$$

For the simple duct shapes, $\alpha_1=12$ for the parallel plates and $\alpha_1=8$ for the circular tubes.

$$A_{ij}=\frac{1}{\varphi_i^2+\psi_j^2}\left\{\frac{4\sin\left(\frac{\varphi_i}{\varepsilon}\right)\sin\psi_j}{\varphi_i\psi_j}+4A_2\frac{2}{1+\varepsilon}Kn^{*}\left[\frac{\sin\left(\frac{\varphi_i}{\varepsilon}\right)\cos\psi_j}{\varphi_i}+\frac{\cos\left(\frac{\varphi_i}{\varepsilon}\right)\sin\psi_j}{\psi_j}\right]\right\}$$
$$\times\left\{\left[\frac{1}{\varepsilon}+\frac{\sin\left(\frac{2\varphi_i}{\varepsilon}\right)}{2\varphi_i}\right]\left(1+\frac{\sin 2\psi_j}{2\psi_j}\right)+2A_2\frac{2}{1+\varepsilon}Kn^{*}\left(\cos^2\psi_j\left[\frac{1}{\varepsilon}+\frac{\sin\left(\frac{2\varphi_i}{\varepsilon}\right)}{2\varphi_i}\right]+\cos^2\left(\frac{\varphi_i}{\varepsilon}\right)\left(1+\frac{\sin 2\psi_j}{2\psi_j}\right)\right)\right\}^{-1} \tag{9}$$

The complete expression of the second-order velocity distribution is complex and space consuming and the analytical procedure will not be repeated here. Details can be found in Aubert and Colin (2001). Upon obtaining the second-order velocity distribution $w(x, y)$ and mean velocity $\bar{w}$, the friction factor and Reynolds number product can be obtained

$$fRe_{\sqrt{A}}=\frac{2\left(-\frac{A}{P}\frac{\mathrm{d}p}{\mathrm{d}z}\right)\sqrt{A}}{\mu\bar{w}}=\frac{4}{\sqrt{\varepsilon}(1+\varepsilon)\left[\sum_{i,j=1}^{\infty}A_{ij}\frac{\varepsilon\sin\left(\frac{\varphi_i}{\varepsilon}\right)\sin\psi_j}{\varphi_i\psi_j}+2A_2\frac{4}{(1+\varepsilon)^2}Kn^{*2}\right]} \tag{10}$$

The Poiseuille number reduction depends on the geometry of the cross section and rarefaction. It is convenient to express the Poiseuille number results by the following relation:

$$\frac{Po_{\mathcal{L}}}{(Po_{\mathcal{L}})_{\mathrm{ns}}}=\frac{fRe_{\mathcal{L}}}{(fRe_{\mathcal{L}})_{\mathrm{ns}}}=\frac{1}{1+\alpha_1Kn^{*}+A_2\alpha_2Kn^{*2}} \tag{11}$$

The relationship is applicable to *arbitrary* length scale (e.g. D_{h}, $\sqrt{A}$) because it cancels. One can use the customary D_{h} if the value of $(fRe_{D_{\mathrm{h}}})_{\mathrm{ns}}$ is known. When the second-order terms can be neglected, Eq. 11 reduces to the first-order model (Duan and Muzychka 2007a):

$$\frac{Po_{\mathcal{L}}}{(Po_{\mathcal{L}})_{\mathrm{ns}}}=\frac{fRe_{\mathcal{L}}}{(fRe_{\mathcal{L}})_{\mathrm{ns}}}=\frac{1}{1+\alpha_1Kn^{*}} \tag{12}$$

The parameters α_1 are a function of aspect ratio and an accurate correlation was proposed (Duan 2011):

We can solve for $A_2\alpha_2$ given values of Kn^{*} and Po/Po_{ns} from Eq. 11. Thus

$$A_2\alpha_2=\frac{\frac{Po_{\mathrm{ns}}}{Po}-1-\alpha_1Kn^{*}}{Kn^{*2}} \tag{14}$$

The second-order slip coefficient A_2 may be temporarily assumed to have a value of unity for convenience in order to obtain the analytical expression of parameter α_2. The same procedure is valid even if $A_2\neq 1$ since the product of $A_2\alpha_2$ is a constant for a specified geometry and rarefaction (Kn^{*}). It is clear that the accurate value of the second-order slip coefficient A_2 requires comparison with precise experimental data, which do not currently exist for various noncircular geometries. The early work by Sreekanth (1969) on low pressure circular tube flow demonstrated that the second-order slip coefficient A_2 has a value of 0.14 for nitrogen. The recent experimental work by Maurer et al. (2003) on silicon microchannels determined a value of 0.26 ± 0.1 for nitrogen and 0.23 ± 0.1 for helium. It is noted that the values of A_2 are derived from mass flow rate measurements and not from direct observations of slip velocity.

The parameters α_2 are a function of aspect ratio and the data points are fitted to a simple correlation as follows:

$$\alpha_2=48-112.7\varepsilon+194.2\varepsilon^2-155.7\varepsilon^3+42.66\varepsilon^4 \tag{15}$$

It is found that the maximum error caused by using these values in Eq. 15 is less than 1.8%. Therefore, using the simple expression Eq. 11, the Poiseuille number results can be easily obtained to facilitate practical application for almost all common circular and noncircular microchannels and nanochannels as follows:

$$fRe_{\sqrt{A}} = \frac{1}{1 + \alpha_1 Kn^* + A_2\alpha_2 Kn^{*2}} \frac{12}{\sqrt{\varepsilon}(1+\varepsilon)\left[1 - \frac{192\varepsilon}{\pi^5}\left(\tanh\left(\frac{\pi}{2\varepsilon}\right) + \frac{1}{243}\tanh\left(\frac{3\pi}{2\varepsilon}\right)\right)\right]} \tag{16}$$

The maximum difference between the analytical solution of Eq. 10 and simple model of Eq. 16 is less than 1.2%.

The effects of slip are illustrated clearly by Fig. 1 which plots the normalized Poiseuille number results as a function of aspect ratio and the modified Knudsen number. It is noted that there are large discrepancies on the value of the second-order slip coefficient which is approximately between -0.5 and 1.1 in the literature. The possible explanation is the second-order slip coefficient is rarefaction (Kn^*) dependent and geometry-dependent. The present choice $A_2 = 0.3$ is only roughly consistent with experimental results of Sreekanth (1969), Hsia and Domoto (1983), Mitsuya (1993), Maurer et al. (2003), Ewart et al. (2006, 2007a), and analytical results of Hadjiconstantinou (2006) and Lockerby et al. (2004). It is seen that the normalized Poiseuille number decreases with an increase in the modified Knudsen number for all aspect ratios. The normalized Poiseuille number decreases more significantly for smaller aspect ratio possibly due to the larger average wall velocity gradients. Figure 1 also illustrates that second-order slip terms become gradually significant with an increase in the modified Knudsen number and the Poiseuille number is overestimated when the second-order terms are not taken into account. This is consistent with the experimental results of Sreekanth (1969), Maurer et al. (2003), Colin et al. (2004), and Ewart et al. (2006, 2007a).

Rij et al. (2009) numerically investigated the frictional and heat transfer characteristics of rarified flows in rectangular microchannels with the second-order slip boundary conditions. The numerical results for the Poiseuille number were calculated using a continuum-based CFD algorithm modified with slip boundary conditions. The normalized Poiseuille number results for the second-order Deissler slip boundary conditions ($A_2 = 9/8$) were presented for different aspect ratios. Figure 2 demonstrates the comparison between the proposed model and Rij et al. (2009) numerical data for different aspect ratios rectangular microchannels. The model is in agreement with data from Van Rij et al. within 1.5%.

Wang (2003a) presented an exact solution for the slip flow in an equilateral triangle. The slip condition invalidates almost all conformal mapping techniques and the exact solutions for other relatively complex noncircular geometries do not exist. Semi-numerical methods were employed for slip flow in other duct cross sections. Wang (2003b) studied slip flow in several noncircular ducts by eigenfunction expansion and point match. The eigenfunction

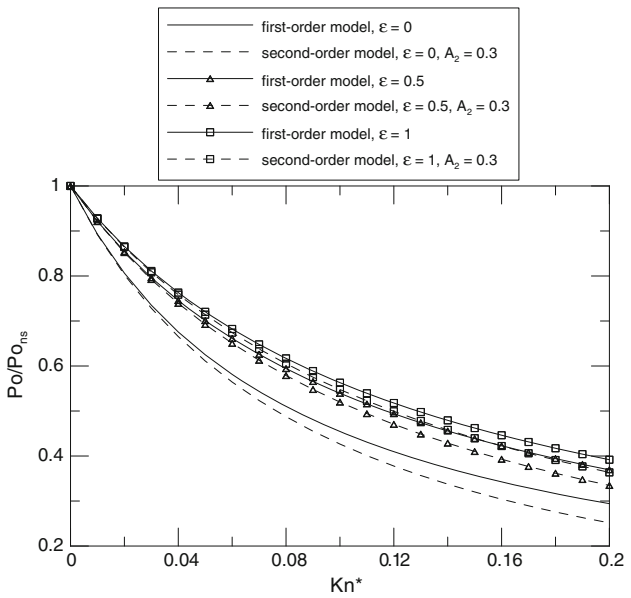

Fig. 1 Effect of second-order slip boundary conditions on normalized Poiseuille number

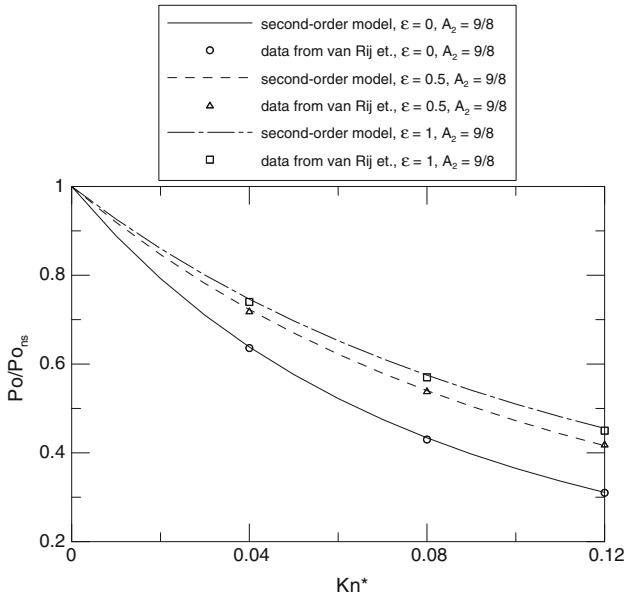

Fig. 2 Comparison of normalized Poiseuille number for the numerical data from Rij et al. (2009)

expansion and point match is a technique to obtain approximate solutions to Dirichlet's problem by fitting a linear combination of a finite number of harmonic functions (each harmonic function is a solution to Laplace's equation) to the specified boundary conditions. Zhu et al. (2006) used eigenfunction and integration which is similar to a Ritz method. These approaches are general, applicable to many irregular configurations although the procedure is relatively complex and lengthy. Hooman (2008) also proposed an approximate superposition approach for several noncircular microchannels.

Morini et al. (2005) numerically studied the velocity distribution in microchannels with trapezoidal (with an apex angle $\omega = 54.74°$ imposed by the crystallographic morphology of the <100> silicon) and hexagonal (double-trapezoidal obtained by gluing together two trapezoidal channels) cross section typical of microchannels. For the trapezoidal microchannels, the aspect ratio b/a cannot exceed the value of $tg(\omega)/2$, corresponding to the degeneration of the isosceles triangular ducts. In the case of a double-trapezoidal cross section, the aspect ratio b/a ranges between 0 (parallel plates) and 1.414 (rhombic configuration). The channel height was employed as the length scale to define the Knudsen number. The corresponding value of α for trapezoidal and double-trapezoidal microchannels was numerically determined and reported for different aspect ratios.

Niazmand et al. (2008) numerically investigated slip flow and heat transfer in trapezoidal microchannels. A specified range of channel aspect ratios and side angles ($\omega = 30°, 45°, 60°, 90°$) are considered. The fully developed values of the friction coefficients as a function of Knudsen number are reported for different side angles and aspect ratios.

Varoutis et al. (2009) performed a numerical and experimental study of gas flows through long channels of rectangular, equilateral triangular, trapezoidal cross sections in the whole range of the Knudsen number from the free molecular, through the transition and slip regimes up to the continuum regime. The numerical approach is based on the solution of the Bhatnagar–Gross–Krook kinetic equation subject to Maxwell diffuse-specular boundary conditions.

Shams et al. (2009) numerically examined fully developed slip flow in rhombus microchannels for different aspect ratio ($0.15 < b/a < 1$). The momentum and energy equations were solved by a finite volume method. The effects of Knudsen number and channel aspect ratio on Poiseuille number were reported.

The simple model of Eq. 11 can be applied to other common geometries with first-order slip boundary conditions, which are available in the literature. Figure 3 presents the comparison between the proposed model of Eq. 11 and the analytical solution of elliptic ducts (Duan and Muzychka 2007b), rectangular and annular ducts

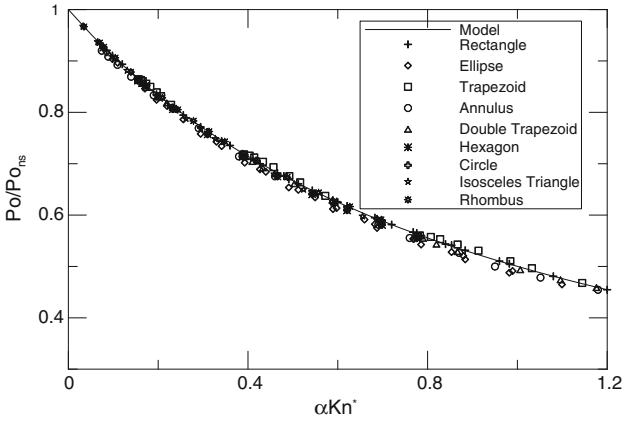

Fig. 3 Comparison of the model for noncircular microchannels

(Duan and Muzychka 2007a), equilateral triangular ducts (Wang 2003a), the numerical data of isosceles triangular, rhombic, trapezoidal, double-trapezoidal and hexagonal ducts (Morini et al. 2005), numerical data of trapezoidal ducts for different side angles and aspect ratios (Niazmand et al. 2008), numerical data of rectangular, equilateral triangular, trapezoidal ducts (Varoutis et al. 2009), and numerical results of rhombus ducts (Shams et al. 2009). The model predictions are in agreement with all the available slip flow data within 3.0%.

4 Flow rate and pressure distribution

As it is quite difficult to solve the Navier–Stokes equations to determine the actual velocity distribution of the compressible rarefied gas flow in noncircular microchannels, the flow is assumed to be locally fully developed and approximately isothermal. Compressibility effects enter through state equation and continuity equation. In the following analysis for the pressure distribution and mass flow rate in microchannel flows, momentum changes are neglected as the pressure force is mostly utilized to overcome the friction force against the walls, very little is spent in accelerating the flow. The effects of the momentum changes due to gas acceleration along the channel will become gradually important when Mach number is increased. Therefore, when the outlet Mach number is larger than 0.3, the momentum flux correction should be taken into consideration. Details can be found in Duan (2007) and Duan and Muzychka (2007c).

4.1 Mass flow rate

The mass flow rate in the microchannel is given by using the equation of state $p = \rho RT$, and the developed simple model of Eq. 11 (of course, one can also use other length

scales such as customary D_h if the value of $(fRe_{D_h})_{ns}$ is known). Combining these expressions yields:

$$\dot{m} = \rho\bar{w}A = \rho A \frac{2\left(-\frac{A}{P}\frac{dp}{dz}\right)\sqrt{A}}{\mu f Re_{\sqrt{A}}} = -\frac{2\frac{A}{P}A\sqrt{A}}{\mu RT\left(fRe_{\sqrt{A}}\right)_{ns}}\frac{dp}{dz}p\left(1+\alpha_1 Kn^* + A_2\alpha_2 Kn^{*2}\right) \quad (17)$$

We can use $pKn = p_o Kn_o$ from the kinetic theory of gases since pKn is constant for isothermal flow. Integrating Eq. 17 from $z = 0$ to local position $z = z$, we obtain

$$\dot{m} = \rho\bar{w}A = \frac{p_o^2\frac{A^{5/2}}{P}}{\mu RTz\left(fRe_{\sqrt{A}}\right)_{ns}} \times \left[\frac{p_i^2}{p_o^2} - \frac{p_z^2}{p_o^2} + 2\alpha_1 Kn_o^*\left(\frac{p_i}{p_o} - \frac{p_z}{p_o}\right) + 2A_2\alpha_2 Kn_o^{*2}\ln\frac{p_i}{p_z}\right] \quad (18)$$

Letting $z = L$ gives:

$$\dot{m} = \rho\bar{w}A = \frac{p_o^2\frac{A^{5/2}}{P}}{\mu RTL\left(fRe_{\sqrt{A}}\right)_{ns}}\left[\frac{p_i^2}{p_o^2} - 1 + 2\alpha_1 Kn_o^*\left(\frac{p_i}{p_o} - 1\right) + 2A_2\alpha_2 Kn_o^{*2}\ln\frac{p_i}{p_o}\right] \quad (19)$$

It can be demonstrated that the limit of Eq. 19 for $\varepsilon \to 0$ corresponds to parallel plates channel

$$\dot{m} = \frac{2ab^3p_o^2}{3\mu RTL}\left[\frac{p_i^2}{p_o^2} - 1 + 24Kn_o^*\left(\frac{p_i}{p_o} - 1\right) + 96A_2Kn_o^{*2}\ln\frac{p_i}{p_o}\right] \quad (20)$$

Also, the limit of Eq. 19 for $\varepsilon \to 1$ approximately reduces to circular tubes

$$\dot{m} = \frac{\pi D^4 p_o^2}{256\mu RTL}\left[\frac{p_i^2}{p_o^2} - 1 + 16Kn_o^*\left(\frac{p_i}{p_o} - 1\right) + 32A_2Kn_o^{*2}\ln\frac{p_i}{p_o}\right] \quad (21)$$

It is convenient to define the dimensionless mass flow rate as

$$m^* = \frac{\dot{m}\mu RTL\left(fRe_{\sqrt{A}}\right)_{ns}}{p_o^2\frac{A^{5/2}}{P}} = \left[\frac{p_i^2}{p_o^2} - 1 + 2\alpha_1 Kn_o^*\left(\frac{p_i}{p_o} - 1\right) + 2A_2\alpha_2 Kn_o^{*2}\ln\frac{p_i}{p_o}\right] = \frac{2\Delta p}{p_o}\left(1 + \frac{\Delta p}{2p_o} + \alpha Kn_o^* + A_2\alpha_2 Kn_o^{*2}\frac{\ln\left(1+\frac{\Delta p}{p_o}\right)}{\frac{\Delta p}{p_o}}\right) \quad (22)$$

When the parameter $\Delta p/p_o \ll 1$, the effect of compressibility is negligible. When $Kn_o^* \ll 1$, then the rarefaction effect is negligible. When both parameters are sufficiently small, the general relation becomes

$$\dot{m} = \rho\bar{w}A = \frac{2\rho A^{5/2}\Delta p}{\mu PL\left(fRe_{\sqrt{A}}\right)_{ns}} \quad (23)$$

which is the relation for flow of an incompressible fluid without slip.

The mass flow rate model of Eq. 22 has been examined using experimental data of Arkilic et al. (1997). Figure 4 presents the normalized mass flow rate of Eq. 22 as a function of the pressure ratio. It is found that the predictions agree with experimental data by Arkilic et al. within 7.8%. The maximum deviation occurs for small pressure ratios, which may be due to experimental errors. An excellent agreement between the second-order model and experimental results is obtained by choosing the second-order slip coefficient $A_2 = 0.3$. Furthermore, the choice $A_2 = 0.3$ is approximately consistent with experimental results of Sreekanth (1969), Hsia and Domoto (1983), Mitsuya (1993), Maurer et al. (2003), and Ewart et al. (2006, 2007a). For comparative purposes the theoretical curve for $Kn = 0$ is shown. It is seen from this figure that there is a significant mass flow rate increase due to rarefaction effects. The experimental data and model predictions are in good agreement.

The no-slip mass flow rate is given from Eq. 19

$$\dot{m}_{ns} = \rho\bar{w}A = \frac{p_o^2\frac{A^{5/2}}{P}}{\mu RTL\left(fRe_{\sqrt{A}}\right)_{ns}}\left(\frac{p_i^2}{p_o^2} - 1\right) \quad (24)$$

The effect of rarefaction may be illustrated clearly by dividing the mass flow rate of Eq. 19 by the no-slip mass flow rate of Eq. 24

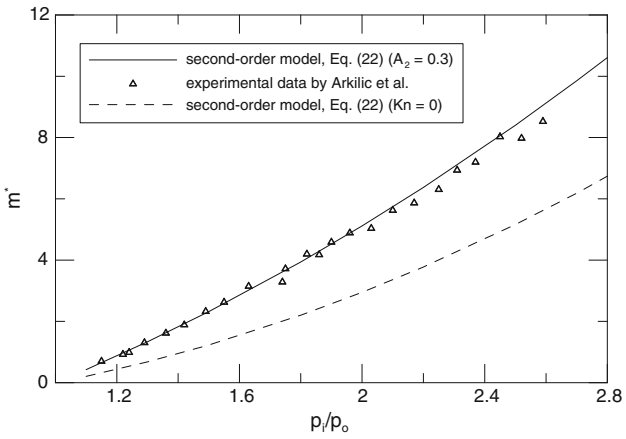

Fig. 4 Normalized mass flow rate comparison of experimental data by Arkilic et al. (1997)

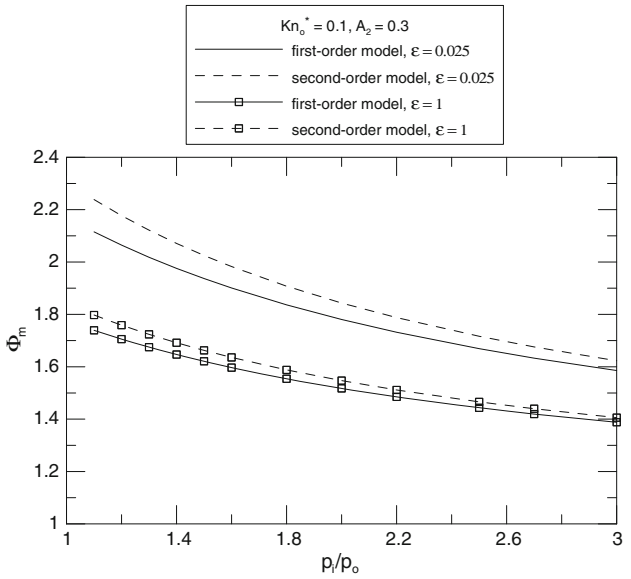

Fig. 5 Mass flow rate ratio for the different aspect ratios

$$\Phi_m = \frac{\dot{m}}{\dot{m}_{\mathrm{ns}}} = 1 + \frac{2\alpha_1 Kn_o^*}{\frac{p_i}{p_o} + 1} + \frac{2A_2\alpha_2 Kn_o^{*2} \ln\frac{p_i}{p_o}}{\frac{p_i^2}{p_o^2} - 1} \tag{25}$$

Figure 5 shows the mass flow rate ratio as a function of the inlet and outlet pressure ratio. The outlet modified Knudsen number Kn_o^* is equal to 0.1, and two typical values of the aspect ratio are considered ($\varepsilon = 0.025$ is close to parallel plates). Figure 5 demonstrates that the mass flow rate is underpredicted when the second-order terms are not taken into account. This result is in agreement with precious studies for rarefied gas flows by Sreekanth (1969), Mitsuya (1993), Maurer et al. (2003), Colin et al. (2004), Ewart et al. (2006, 2007a). It is seen that the rarefaction increases the mass flow rate.

4.2 Pressure distribution

The local pressure ratio can be related to the inlet and outlet pressure ratio and the local relative position. Combining Eqs. 18 and 19 and solving for p_z/p_o, we obtain the implicit expression for pressure distribution in noncircular microchannels:

$$\frac{p_i^2}{p_o^2} - \frac{p_z^2}{p_o^2} + 2\alpha_1 Kn_o^*\left(\frac{p_i}{p_o} - \frac{p_z}{p_o}\right) + 2A_2\alpha_2 Kn_o^{*2}\ln\frac{p_i}{p_z} = \frac{z}{L}\left[\frac{p_i^2}{p_o^2} - 1 + 2\alpha_1 Kn_o^*\left(\frac{p_i}{p_o} - 1\right) + 2A_2\alpha_2 Kn_o^{*2}\ln\frac{p_i}{p_o}\right] \tag{26}$$

Upon obtaining the pressure distribution p_z/p_o, the deviations of the nonlinear pressure distribution from the linear distribution is given by:

$$\frac{p_z - p_{\mathrm{linear}}}{p_o} = \frac{p_z}{p_o} - \left[\frac{p_i}{p_o} - \left(\frac{p_i}{p_o} - 1\right)\frac{z}{L}\right] \tag{27}$$

Taking the derivative of Eq. 27 and setting it equal to zero, the location of the maximum deviation from linearity can be obtained. The typical location of maximum deviation from linearity is between 0.5 and 0.6 for practical applications (moderate inlet and outlet pressure ratios) (Duan 2007).

When the second-order terms can be neglected, Eq. 26 reduces to the following explicit form for pressure distribution (Duan and Muzychka 2007a):

$$\frac{p_z}{p_o} = -\alpha_1 Kn_o^* + \sqrt{\left(\alpha_1 Kn_o^* + \frac{p_i}{p_o}\right)^2 - \left[\frac{p_i^2}{p_o^2} - 1 + 2\alpha_1 Kn_o^*\left(\frac{p_i}{p_o} - 1\right)\right]\frac{z}{L}} \tag{28}$$

It is seen from Eq. 28 that the pressure distribution is insensitive and nearly independent of various geometries at the same inlet and outlet pressure ratio. Figure 6 presents the pressure distribution for different slip boundary conditions. The analytical pressure distribution with the second-order slip boundary conditions has lower values than those from first-order case. The pressure distribution is overestimated if only first-order terms are considered. However, the difference between the first-order and second-order is not very significant. The difference increases with an increase in the Knudsen number.

The pressure distribution applies to circular and noncircular microchannels through the dimensionless parameters α, Kn_o^*, p_i/p_o. The pressure distribution exhibits a nonlinear behavior due to the compressibility effect. The deviations of the pressure distribution from the linear distribution decrease with an increase in the Knudsen number. The nonlinearity increases as the pressure ratio increases. The nonlinearity decreases if the second-order terms are

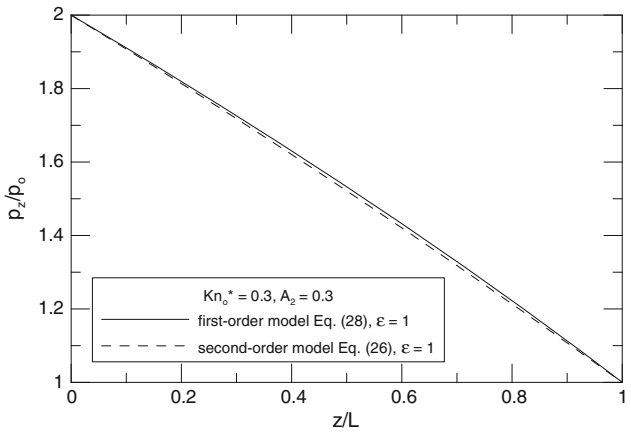

Fig. 6 Pressure distribution for different models

taken into account. The effects of compressibility and rarefaction are opposite as Karniadakis et al. (2005) and Kandlikar et al. (2006) demonstrated. When the pressure ratio is very small, the pressure distribution is nearly linear, which is close to an incompressible flow.

Karniadakis et al. (2005) simulated nitrogen flow in a long microchannel which is 1.25 μm high and 40 μm wide. Figure 7 shows the deviation from linear pressure distribution comparison between the proposed second-order model of Eq. 27 and numerical simulation results by Karniadakis et al. Eq. 27 agrees with simulation results by Karniadakis et al. (2005) very well.

It is well known that the curvature of the pressure distribution is convex. Nevertheless, it is noteworthy from second-order model of Eq. 26 that the curvature of the pressure distribution gradually changes from widely known convex to concave with an increase in the Knudsen number. This phenomenon has also been observed in the lattice-Boltzmann simulations of fluid flows in MEMS by Nie et al. (2002). This peculiar phenomenon requires further experimental validation. Taking the derivative of Eq. 26 twice with respect to z and setting d^2p_z/dz^2 equal to zero, the condition of zero curvature (linear) of the pressure distribution can be obtained as

$$\frac{p_z^2}{p_o^2} - A_2\alpha_2 Kn_o^{*2} = 0 \tag{29}$$

It is seen that the curvature is always convex by using the first-order model since Eq. 29 ($p_z/p_o = 0$) cannot be satisfied. Equation 26 also clearly theoretically explains the reason why the pressure distribution exhibits a nonlinear behavior due to the compressibility effect and the pressure distribution (p_z/p_o) approaches the linear asymptote with a decrease in the pressure ratio but cannot be really linear by using the first-order model. It is well known that at higher Knudsen number the curvature in the pressure distribution is much smaller, with linear pressure distribution observed as $Kn > 10$ (Knudsen 1909; Kennard 1938; Karniadakis et al. 2005). Therefore, Eq. 29 further indicates that at very large Knudsen number the second-order slip coefficient A_2 should gradually decrease with an increase of the Kundsen number.

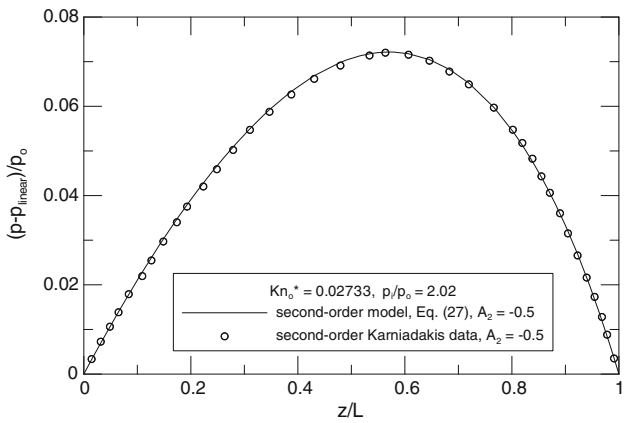

Fig. 7 Deviation from linear pressure distribution comparison for second-order numerical data from Karniadakis et al. (2005)

It is also widely known from experiments in the transition regime by Knudsen (1909) that there is a minimum in the flow rate in channel flows at $Kn \approx 0.5$. Note that the hydraulic diameter is employed as the characteristic length scale used to define the Knudsen number in the present study. If the channel height is used as the characteristic length scale to define the Knudsen number, $Kn \approx 1$. This peculiar behavior has been studied by many researchers both theoretically and experimentally (Cercignani and Daneri 1963; Tison 1993; Karniadakis et al. 2005; Hadjiconstantinou 2006; Ewart et al. 2007b; Marino 2009; Pitakarnnop et al. 2010; Perrier et al. 2011). The volumetric flow rate is presented at the Knudsen number in the channel (corresponding to the pressure p). The dimensionless volumetric flow rate for arbitrary Knudsen numbers is obtained as:

$$\bar{Q} = \frac{\dot{Q}p}{-\frac{dp}{dz}(2b)^2\sqrt{\frac{RT}{2}}} = \frac{\bar{w}2bp}{-\frac{dp}{dz}(2b)^2\sqrt{\frac{RT}{2}}} = \frac{\bar{w}p}{-\frac{dp}{dz}2b\sqrt{\frac{RT}{2}}} \tag{30}$$

where $\dot{Q}$ is the volumetric flow rate per unit width of the channel. After substitution for $\bar{w}$ and using Eq. 11 we obtain the following relation:

$$\begin{aligned}\bar{Q} &= \frac{p}{-\frac{dp}{dz}2b\sqrt{\frac{RT}{2}}}\frac{2\left(-\frac{A}{P}\frac{dp}{dz}\right)D_h}{\mu f Re_{D_h}} \\ &= \frac{p}{2b\sqrt{\frac{RT}{2}}}\frac{2\frac{A}{P}D_h}{\mu(fRe_{D_h})_{ns}}\left(1+\alpha_1 Kn^* + A_2\alpha_2 Kn^{*2}\right)\end{aligned} \tag{31}$$

Multiplying by Kn^*/Kn^*, we obtain

$$\begin{aligned}\bar{Q} &= \frac{pKn^*}{2b\sqrt{\frac{RT}{2}}}\frac{2\frac{A}{P}D_h}{\mu(fRe_{D_h})_{ns}}\frac{1+\alpha_1 Kn^* + A_2\alpha_2 Kn^{*2}}{Kn^*} \\ &= C\left(\frac{1}{Kn^*} + \alpha_1 + A_2\alpha_2 Kn^*\right)\end{aligned} \tag{32}$$

Because the dimensionless volumetric flow rate $\bar{Q} = \bar{Q}(Kn)$ in the transition regime varies slowly about its minimum value at $Kn \approx 0.5$ as seen from experimental data of Dong (Cercignani and Daneri 1963), Tison (1993), Ewart et al. (2007b), Marino (2009), and Perrier et al. (2011), the Knudsen's minimum is not very sensitive to the choice of second-order slip coefficient A_2. It is seen that the Knudsen's minimum can be predicted with the second-order model by choosing the appropriate second-order slip coefficient ($A_2 \cong 0.083$ for parallel plates by differentiating Eq. 32 with respect to Kn^* and letting it equal to zero. As mentioned

above, since the Knudsen's minimum is insensitive to the selection of second-order slip coefficient, $A_2 \cong 0.05 \sim 0.3$). Furthermore, it is worth noting from Knudsen's experiment that the nondimensionalized volumetric flow rate data are presented at the mean pressure between the inlet and outlet in the channel (corresponding to the average Knudsen number). Therefore, the Knudsen value of the occurrence of Knudsen's minimum is really *approximately* equal to 1 and should depend on the pressure ratio and the effective aspect ratio. The Knudsen number of the occurrence of Knudsen's minimum decreases with a decrease in the pressure ratio. Equation 32 analytically indicates that the Knudsen's discovery can be captured by the Navier–Stokes equations with second-order slip boundary conditions. This is consistent with the conclusion of Karniadakis et al. (2005), Hadjiconstantinou (2006), and Dongari et al. (2007) for parallel plates. Navier–Stokes equations with second-order slip model can be used to simulate a relatively large range of Knudsen number. It is also noticed from Eq. 32 that if the first-order slip model is used, the dimensionless volumetric flow rate decreases monotonically with an increase of the Knudsen number. Therefore, the Knudsen's minimum cannot be captured by employing the first-order slip model.

Knudsen found that the dimensionless volumetric flow rate $\bar{Q}$ approached to a constant value in the free molecular flow regime (Knudsen 1909; Kennard 1938; Karniadakis et al. 2005). This means by examining Eq. 32 that the value of $A_2 Kn^*$ asymptotically approaches a constant value in the free molecular flow regime. Therefore, Eq. 32 once again indicates that the second-order slip coefficient A_2 should gradually decrease with an increase of the Kundsen number at very large Knudsen numbers.

In the transition regime, the available experimental data are quite insufficient. Moreover, there is uncertainty about the exactitude of the available data from limited different sources. A simple model based on the available experimental data (Sreekanth 1969; Maurer et al. 2003; Colin et al. 2004; Ewart et al. 2006, 2007a, b; Varoutis et al. 2009; Pitakarnnop et al. 2010; Perrier et al. 2011; Fissell et al. 2011), the Boltzmann solution (Ohwada et al. 1989), the solution of the BGK model kinetic equation (Loyalka 1975; Loyalka et al. 1976; Sharipov and Seleznev 1998; Sharipov 1999), and DSMC simulation results (Karniadakis et al. 2005) for gas flows through long circular, parallel plates, rectangular, triangular, trapezoidal, elliptical channels in the literature is proposed as a quite accurate approximation of A_2 in the transition regime:

$$A_2 = 0.185 - 0.127\ln(Kn^*) + 0.0388(\ln(Kn^*))^2 - 0.00435(\ln(Kn^*))^3 \quad (33)$$

For example, Fig. 8 shows the dimensionless flow rate comparison between the proposed second-order model $\left[\text{for parallel plates,}\quad \bar{Q} = \frac{\sqrt{\pi}}{24}\left(\frac{1}{Kn} + 12 + 48A_2 Kn\right)\right]$ and the solution of the linearized Boltzmann equation for a hard-sphere gas (Ohwada et al. 1989), experimental data from Ewart et al. (2007b) (the aspect ratio is 0.019), the numerical solution of the BGK model associated with a Maxwell diffuse-specular reflection law (Loyalka 1975), and the numerical solution of the BGK model equation in the rectangular channel with an aspect ratio of 0.01 (Sharipov 1999), where the rarefaction parameter δ is inversely proportional to the Knudsen number. The second-order model performs quite well in the transition regime even further bordering the free molecular regime. As shown in Fig. 8, the dimensionless flow rate in the transition regime varies slowly about its minimum value.

Very few measurements on rarefied gas flow through rectangular channels have been made. Rarefied gas flow

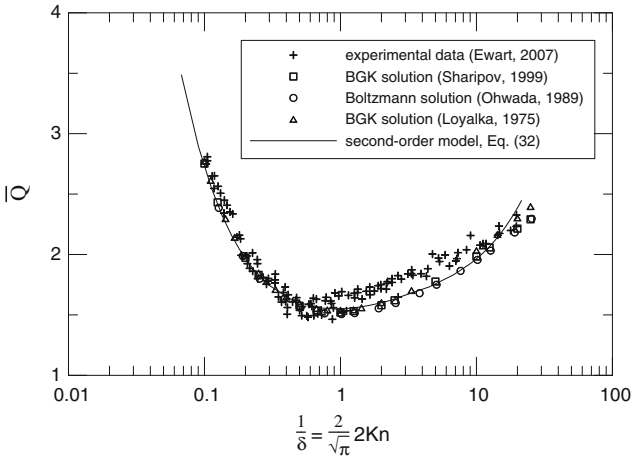

Fig. 8 Nondimensional flow rate as a function of the Knudsen number

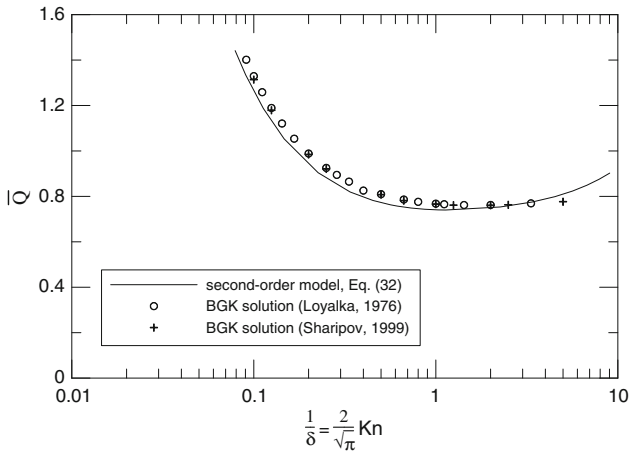

Fig. 9 Nondimensional flow rate as a function of the Knudsen number in a square channel

through a long square channel are computed using the BGK model of the Boltzmann equation and diffuse scattering from the walls (Loyalka et al. 1976; Sharipov 1999). The proposed second-order model [for a square channel, $\bar{Q} = \frac{\sqrt{\pi}}{2\times 14.227}\left(\frac{1}{Kn} + 7.83 + 16.46A_2Kn\right)$] is compared with the available numerical data as shown in Fig. 9. It is seen that the Knudsen minimum exists in the transition regime at any aspect ratio. The present work provides a simple and accurate way to compute rarefied gas flow in a channel.

5 Conclusion

This paper investigated gaseous flow in noncircular microchannels. It extended previous studies to the transition regime by employing the second-order slip boundary conditions for gaseous flows in microchannels. A simple model for the normalized Poiseuille number was developed. The accuracy of the developed model for the normalized Poiseuille number was found to be within 3% for all common duct shapes which are available in the literature. As in slip and transition regimes no solutions or tabulated data exist for most geometries, this developed model fills this void. This developed model can be used to easily predict the Poiseuille number, mass flow rate, tangential momentum accommodation coefficient, pressure distribution, and pressure drop (Duan 2011) of gaseous flow in circular and noncircular microchannels such as rectangular, trapezoidal, double-trapezoidal, triangular, rhombic, hexagonal, octagonal, elliptical, semielliptical, parabolic, circular sector, circular segment, annular sector, rectangular duct with unilateral elliptical or circular end, annular, and even comparatively complex bent microducts and nanoducts. The model for normalized Poiseuille number can also be utilized to predict Poiseuille number, flow rate, and pressure drop for liquid slip flow in nanochannels. The shape dependence has been minimized and can be nearly neglected for the practical engineering design. This weak shape dependence is valuable because perfect channels are rarely achieved in engineering practice. The similar method can be applied to associated gaseous flow heat transfer problem in the future work. It is noteworthy that the developed model for the normalized Poiseuille number is *independent* of the characteristic length scale used to define the Reynolds number.

It has been shown that the Poiseuille number is overestimated and the mass flow rate is underpredicted when the second-order terms are not taken into account. The Knudsen's minimum can be predicted with the second-order model and cannot be captured by only employing the first-order slip model. The Knudsen number of the occurrence of Knudsen's minimum decreases with a decrease in the inlet and outlet pressure ratio. The compressibility and rarefaction effects on mass flow rate and the curvature of the pressure distribution by employing first-order and second-order slip flow models are analyzed and compared. The reason why the pressure distribution exhibits a nonlinear behavior is theoretically explained. The condition of linear pressure distribution is given. The developed second-order slip flow models can be reduced to the first-order models by neglecting the second-order terms.

It is noted that there are large divergences on the value of the second-order slip coefficient which is typically approximately between 0.1 and 1.1. It is reasonable that the second-order slip coefficient is positive because the Knudsen's minimum cannot be captured by Eq. 32 if $A_2 \leq 0$. It is apparent that there is a need for precise experimental data in a wider range of the Knudsen number to address the measurement of the velocity profile within the Knudsen layer. Experimental velocity data in the wall adjacent layer would be invaluable in helping choose appropriate second-order slip coefficients. Also, there is a clear need for experimental investigations in order to determine whether the second-order slip coefficient is Knudsen number (rarefaction) dependent and geometry-dependent. These experimental results will help explain the reason why there are large differences on the value of the second-order slip coefficient. It should be reasonable (not strange) that various researchers proposed different second-order slip coefficients because the values are naturally different in different Knudsen number regimes. The second-order slip coefficient A_2 should smoothly vary (increase) from widely known nearly zero in the slip regime to an appropriate value (approximately 0.3–0.5 based on limited experimental data (Sreekanth 1969; Maurer et al. 2003; Colin et al. 2004; Ewart et al. 2006, 2007a, b; Varoutis et al. 2009; Perrier et al. 2011; Fissell et al. 2011 and most theoretical results) in the transition regime, and then gradually decrease and approach zero with an increase of the Kundsen number as indicated from Eqs. 29 and 32. In other words, maybe there is a maximum in second-order slip coefficient A_2 near the boundaries between slip and transition regime. It could be rational since the transition regime is a varying mixture of different transport mechanisms and the mixed degree relies on the magnitude of the Knudsen number.

Extending the range of applicability of the Navier–Stokes equations beyond the first-order slip flow is desirable due to the simplicity and significant computational efficiency. Navier–Stokes equations with second-order slip models can be used to predict quantities of engineering interest such as Poiseuille number, flow rates, pressure distribution, and pressure drop for a large range of Knudsen number. The appropriate or effective second-order slip coefficients include the contribution of the Knudsen layers

in order to capture the complete solution of the Boltzmann equation for the mass flow rate (Hadjiconstantinou 2006; Sone 2007; Cercignani and Lorenzani 2010; Lorenzani 2011; Karniadakis et al. 2005). The appropriate or effective second-order slip coefficients can provide accurate average velocity and capture many nonequilibrium effects in the transition regime as shown in Figs. 8 and 9. To conveniently bridge kinetic theory and conventional fluid dynamics in the transition regime is completely possible.

The extension of the second order in the high Knudsen number regime is a scientific speculation without strictly theoretical proof since theoretical verification is an extremely hard task. However, the well-founded second-order slip coefficient A_2 is not constant and gradually decreases and approach zero with an increase of the Kundsen number. The appropriate or effective second-order slip coefficients can be obtained by comparing the second-order models with experimental data, the Boltzmann solution, DSMC calculation results, BGK simulation results, and other existing theories. The excellent agreement for the mass flow rate can be obtained with experimental data, DSMC calculation results, the Boltzmann solution, BGK simulation results, other theoretical approaches (Sreekanth 1969; Maurer et al. 2003; Colin et al. 2004; Ewart et al. 2006, 2007a, b; Varoutis et al. 2009; Pitakarnnop et al. 2010; Perrier et al. 2011; Fissell et al. 2011; Loyalka 1975; Loyalka et al. 1976; Ohwada et al. 1989; Sharipov and Seleznev 1998; Sharipov 1999; Karniadakis et al. 2005; Hadjiconstantinou 2006; Cercignani and Lorenzani 2010) without involving any kind of complexities. Undoubtedly, the great advantages of the second-order models are remarkable simplicity and distinct computational efficiency. To extend the applicability of the continuum description is significantly more efficient compared to molecular-based approaches.

The theoretical basis and a definitive picture of the transition regime is not very clear. Therefore, the transition regime is the most challenging to model. The experimental study and molecular-based simulation previously have been confined to simple geometries such as circular tubes and parallel plates mainly due to the rarefaction effects, which make this particular gas flow problem even more complicated. A survey of the literature indicates a shortage of information for most noncircular geometries. There currently is no published model for noncircular geometries which can be utilized by the research and design communities. Further experimental verification of the models is strongly required. More realistic models (more appropriate second-order slip coefficients) should be developed in future work if the present models are found to be insufficient.

The developed models are useful for the following reasons: (1) an indication of the effect of various independent parameters such as the tangential momentum accommodation coefficient, the second-order slip coefficient, Knudsen number, pressure ratio, pressure drop, and geometries; (2) a weak function of the duct shape; (3) an indication of trends expected from related numerical data and future experiments; (4) very simple and easy to utilize by the research and design communities (a core objective in engineering practice); and (5) a demonstration that with some relatively simple ideas from knowledge, observation, and intuition, one can predict some fairly complex flows (making the complex simple without losing the essence).

Acknowledgments The author wishes to thank the anonymous reviewers and Dr. Stephane Colin for helpful comments for improvements. The author acknowledges professors Michael Yovanovich, Yuri Muzychka, and Richard Culham, who meant a lot to the work.

References

Agrawal A, Djenidi L, Agrawal A (2009) Simulation of gas flow in microchannels with a single 90 degrees bend. Comput Fluids 38:1629–1637

Araki T, Kim MS, Hiroshi I, Suzuki K (2000) An experimental investigation of gaseous flow characteristics in microchannels. In: Celata GP (ed) Proceedings of international conference on heat transfer and transport phenomena in microscale. Begell House, New York, pp 155–161

Arkilic EB, Breuer KS, Schmidt MA (1994) Gaseous flow in microchannels. In: Application of microfabrication to fluid mechanics, ASME vol. FED-197, pp 57–66

Arkilic EB, Breuer KS, Schmidt MA (1997) Gaseous slip flow in long microchannels. J Microelectromech Syst 6:167–178

Asproulis N, Drikakis D (2010a) Boundary slip dependency on surface stiffness. Phys Rev E 81:061503

Asproulis N, Drikakis D (2010b) Surface roughness effects in micro and nanofluidic devices. J Comput Theor Nanosci 7:1825–1830

Asproulis N, Drikakis D (2011) Wall mass effects on hydrodynamic boundary slip. Phys Rev E 84:031504

Aubert C, Colin S (2001) High-order boundary conditions for gaseous flows in rectangular microducts. Microscale Thermophys Eng 5:41–54

Barber RW, Emerson DR (2006) Challenges in modeling gas-phase flow in microchannels: from slip to transition. Heat Transf Eng 27:3–12

Carslaw HS, Jaeger JC (1959) Conduction of heat in solids, 2nd edn. Oxford University Press, Oxford

Cercignani C (1988) The Boltzmann equation and its applications. Springer, Berlin

Cercignani C, Daneri A (1963) Flow of a rarefied gas between two parallel plates. J Appl Phys 34:3509–3513

Cercignani C, Lorenzani S (2010) Variational derivation of second-order coefficients on the basis of the Boltzmann equation for hard-sphere molecules. Phys Fluids 22:062004

Chakraborty S, Duan ZP, Muzychka YS, Anand KD (2008) Implications of hydrophobic interactions and consequent apparent slip phenomenon on the entrance region transport of liquids through microchannels. Phys Fluids 20:043602

Choi SB, Barron RF, Warrington RO (1991) Fluid flow and heat transfer in microtubes. In: Micromechanical sensors, actuators, and systems, DSC vol. 32, ASME, New York, pp 123–134

Choi CH, Johan K, Westin A, Breuer KS (2003) Apparent slip flow in hydrophilic and hydrophobic microchannels. Phys Fluids 15: 2897–2902

Colin S, Lalonde P, Caen R (2004) Validation of a second-order slip flow model in rectangular microchannels. Heat Transf Eng 25: 23–30

Deissler RG (1964) An analysis of second-order slip flow and temperature-jump boundary conditions for rarefied gases. Int J Heat Mass Transf 7:681–694

Dongari N, Agrawal A, Agrawal A (2007) Analytical solution of gaseous slip flow in long microchannels. Int J Heat Mass Transf 50:3411–3421

Duan ZP (2007) Analysis of slip flow in microchannels. PhD dissertation, Memorial University, St. John's, Newfoundland, Canada

Duan ZP (2011) Incompressible criterion and pressure drop for gaseous slip flow in circular and noncircular microchannels. J Fluid Eng 133:074501

Duan ZP (2012) New correlative models for fully developed turbulent heat and mass transfer in circular and noncircular ducts. J Heat Transf 134:014503

Duan ZP, Muzychka YS (2007a) Slip flow in non-circular microchannels. Microfluid Nanofluid 3:473–484

Duan ZP, Muzychka YS (2007b) Slip flow in elliptic microchannels. Int J Thermal Sci 46:1104–1111

Duan ZP, Muzychka YS (2007c) Compressibility effect on slip flow in non-circular microchannels. Nanoscale Microscale Thermophys Eng 11:259–272

Duan ZP, Muzychka YS (2010) Slip flow in the hydrodynamic entrance region of circular and noncircular microchannels. J Fluid Eng 132:011201

Duan ZP, Yovanovich MM (2010) Models for gaseous slip flow in circular and noncircular microchannels. In: Proceedings of ASME 2010 3rd joint US-European fluids engineering summer meeting and 8th international conference on nanochannels, microchannels, and minichannels, Montreal, Canada, FEDSM-ICNMM2010-30320

Ebert WA, Sparrow EM (1965) Slip flow in rectangular and annular ducts. J Basic Eng 87:1018–1024

Ewart T, Perrier P, Graur I, Meolans JG (2006) Mass flow rate measurements in gas micro flows. Exp Fluids 41:487–498

Ewart T, Perrier P, Graur I, Meolans JG (2007a) Tangential momentum accommodation in microtube. Microfluid Nanofluid 3:689–695

Ewart T, Perrier P, Graur I, Meolans JG (2007b) Mass flow rate measurements in a microchannel, from hydrodynamic to near free molecular regimes. J Fluid Mech 584:337–356

Fissell WH, Conlisk AT, Datta S, Magistrelli JM, Glass JT, Fleischman AJ, Roy S (2011) High Knudsen number fluid flow at near-standard temperature and pressure conditions using precision nanochannels. Microfluid Nanofluid 10:425–433

Gad-el-Hak M (2001) MEMS handbook. CRC Press, Boca Raton

Hadjiconstantinou NG (2006) The limits of Navier–Stokes theory and kinetic extensions for describing small-scale gaseous hydrodynamics. Phys Fluids 18:111301

Harley J, Huang Y, Bau H, Zemel JN (1995) Gas flows in microchannels. J Fluid Mech 284:257–274

Hooman K (2008) A superposition approach to study slip-flow forced convection in straight microchannels of uniform but arbitrary cross-section. Int J Heat Mass Transf 51:3753–3762

Hsia YT, Domoto GA (1983) An experimental investigation of molecular rarefaction effects in gas lubricated bearings at ultra-low clearances. J Lubr Tech 105:120–130

Hsieh SS, Tsai HH, Lin CY, Huang CF, Chieh CM (2004) Gas flow in a long microchannel. Int J Heat Mass Transf 47:3877–3887

Jang J, Wereley ST (2004) Pressure distributions of gaseous slip flow in straight and uniform rectangular microchannels. Microfluid Nanofluid 1:41–51

Jie D, Diao X, Cheong KB, Yong JK (2000) Navier–Stokes simulations of gas flow in micro devices. J Micromech Microeng 10:372–379

Kalweit M, Drikakis D (2008) Multiscale methods for micro/nano flows and materials. J Comput Theor Nanosci 5:1923–1938

Kandlikar SG, Garimella SV, Li D, Colin S, King M (2006) Heat transfer and fluid flow in minichannels and microchannels. Elsevier, Oxford

Karniadakis GE, Beskok A, Aluru N (2005) Microflows and nanoflows. Springer, New York

Kennard EH (1938) Kinetic theory of gases. McGraw-Hill, New York

Knudsen M (1909) Die Gesetze der Molekularstromung und der inneren Reibungsstromung der Gase durch Rohren. Annalen der Physik 28:75–130

Li D (2008) Encyclopedia of microfluidics and nanofluidics. Springer, Berlin

Li JM, Wang BX, Peng XF (2000) 'Wall-adjacent layer' analysis for developed flow laminar heat transfer of gases in microchannels. Int J Heat Mass Transf 43:839–847

Lockerby DA, Reese JM, Emerson DR, Barber RW (2004) Velocity boundary condition at solid walls in rarefied gas calculations. Phys Rev E 70:017303

Lorenzani S (2011) Higher order slip according to the linearized Boltzmann equation with general boundary conditions. Philos Trans R Soc A 369:2228–2236

Loyalka SK (1975) Kinetic theory of thermal transpiration and mechanocaloric effect II. J Chem Phys 63:4054–4060

Loyalka SK, Storvick TS, Park HS (1976) Poiseuille flow and thermal creep flow in long, rectangular channels in the molecular and transition flow regimes. J Vac Sci Technol 13:1188–1192

Marino L (2009) Experiments on rarefied gas flows through tubes. Microfluid Nanofluid 6:109–119

Maurer J, Tabeling P, Joseph P, Willaime H (2003) Second-order slip laws in microchannels for helium and nitrogen. Phys Fluids 15: 2613–2621

Mitsuya Y (1993) Modified Reynolds equation for ultra-thin film gas lubrication using 1.5-order slip-flow model and considering surface accommodation coefficient. J Tribol 115:289–294

Morini GL, Lorenzini M, Spiga M (2005) A criterion for experimental validation of slip-flow models for incompressible rarefied gases through microchannels. Microfluid Nanofluid 1:190–196

Muzychka YS, Yovanovich MM (2002) Laminar flow friction and heat transfer in non-circular ducts and channels: Part I-hydrodynamic problem. Compact heat exchangers. A Festschrift on the 60th birthday of Ramesh K. Shah, Grenoble, France, pp 123–130

Nguyen NT, Wereley ST (2003) Fundamentals and applications of microfluidics. Artech House, London

Niazmand H, Renksizbulut M, Saeedi E (2008) Developing slip flow and heat transfer in trapezoidal microchannels. Int J Heat Mass Transf 51:6126–6135

Nie X, Doolen GD, Chen S (2002) Lattice-Boltzmann simulations of fluid flows in MEMS. J Stat Phys 107:279–289

Ohwada T, Sone Y, Aoki K (1989) Numerical analysis of the Poiseuille and thermal transpiration flows between parallel plates on the basis of the Boltzmann equation for hard-sphere molecules. Phys Fluids A 1:2042–2049

Perrier P, Graur I, Ewart T, Meolans JG (2011) Mass flow rate measurements in microtubes, from hydrodynamic to near free molecular regime. Phys Fluids 23:042004

Pfahler J, Harley J, Bau H, Zemel JN (1990) Gas and liquid transport in small channels. In: Microstructures, sensors and actuators, DSC vol. 19, ASME, New York, pp 149–157

Pitakarnnop J, Varoutis S, Valougeorgis D, Geoffroy S, Baldas L, Colin S (2010) A novel experimental setup for gas microflows. Microfluidics Nanofluidics 8:57–72

Pong K, Ho C, Liu J, Tai Y (1994) Nonlinear pressure distribution in uniform microchannels. In: ASME application of microfabrication to fluid mechanics, vol. FED-197, pp 51–56

Reese JM, Zhang YH (2009) Simulating fluid flows in micro and nano devices: the challenge of non-equilibrium behaviour. J Comput Theor Nanosci 6:2061–2074

Rij J, Ameel T, Harman T (2009) An evaluation of secondary effects on microchannel frictional and convective heat transfer characteristics. Int J Heat Mass Transf 52:2792–2801

Rohsenow WM, Choi HY (1961) Heat, mass, and momentum transfer. Prentice-Hall, New Jersey

Rovenskaya O, Croce G (2010) Numerical analysis of rarefaction and compressibility effects in bend microchannels. In: Proceedings of ASME 2010 3rd joint US-European fluids engineering summer meeting and 8th international conference on nanochannels, microchannels, and minichannels, Montreal, Canada, FEDSM-ICNMM2010-30489

Schaaf SA, Chambre PL (1958) Flow of rarefied gases. Princeton University Press, New Jersey

Shams M, Shojaeian M, Aghanajafi C, Dibaji SAR (2009) Numerical simulation of slip flow through rhombus microchannels. Int Commun Heat Mass Transf 36:1075–1081

Sharipov F (1999) Rarefied gas flow through a long rectangular channel. J Vac Sci Technol A 17:3062–3066

Sharipov F, Seleznev VD (1998) Data on internal rarefied gas flows. J Phys Chem Ref Data 27:657–706

Sone Y (2007) Molecular gas dynamics: theory, techniques and applications. Birkhauser, Boston

Sreekanth AK (1969) Slip flow through long circular tubes. In: Trilling L, Wachman HY (eds) Proceedings of the sixth international symposium on rarefied gas dynamics, Academic Press, pp 667–680

Thompson PA, Troian SM (1997) A general boundary condition for liquid flow at solid surfaces. Nature 389:360–362

Tison SA (1993) Experimental data and theoretical modeling of gas flows through metal capillary leaks. Vacuum 44:1171–1175

Tretheway DC, Meinhart CD (2002) Apparent fluid slip at hydrophobic microchannel walls. Phys Fluids 14:L9–L12

Varoutis S, Naris S, Hauer V, Day C, Valougeorgis D (2009) Computational and experimental study of gas flows through long channels of various cross sections in the whole range of the Knudsen number. J Vac Sci Technol A 27:89–100

Wang CY (2003a) Slip flow in a triangular duct—an exact solution. Z Angew Math Mech 83:629–631

Wang CY (2003b) Slip flow in ducts. Can J Chem Eng 81:1058–1061

Xue H, Fan Q (2000) A new analytic solution of the Navier–Stokes equations for microchannel flows. Microscale Thermophys Eng 4:125–143

Zhu X, Liao Q, Xin MD (2006) Gas flow in microchannel of arbitrary shape in slip flow regime. Nanoscale Microscale Thermophys Eng 10:41–54

Zohar Y, Lee SY, Lee YL, Jiang L, Wong P (2002) Subsonic gas flow in a straight and uniform microchannel. J Fluid Mech 472: 125–151